Nanoscale Research Letters

NANO EXPRESS Open Access

Dielectric Enhancement of Atomic Layer-Deposited $Al_2O_3/ZrO_2/Al_2O_3$ MIM Capacitors by Microwave Annealing

Bao Zhu[1,2], Xiaohan Wu[2], Wen-Jun Liu[2], Shi-Jin Ding[2*], David Wei Zhang[2] and Zhongyong Fan[1*]

Abstract

For metal-insulator-metal (MIM) capacitors applicated in the fields of RF, DRAM, and analog/mixed-signal integrated circuits, a high capacitance density is imperative with the downscaling of the device feature size. In this work, the microwave annealing technique is investigated to enhance the dielectric characteristics of $Al_2O_3/ZrO_2/Al_2O_3$ based MIM capacitors. The results show that the permittivity of ZrO_2 is increased to 41.9 (~ 40% enhanced) with a microwave annealing at 1400 W for 5 min. The substrate temperature is lower than 400 °C, which is compatible with the back end of line process. The leakage current densities are 1.23×10^{-8} and 1.36×10^{-8} A/cm^2 for as-deposited sample and 1400 W sample, respectively, indicating that the leakage property is not deteriorated. The conduction mechanism is confirmed as field-assisted tunneling.

Keywords: Microwave annealing, Atomic layer deposition, $Al_2O_3/ZrO_2/Al_2O_3$, MIM capacitors

Background

Metal-insulator-metal (MIM) capacitors have been widely used in the fields of radio frequency (RF), dynamic random access memory (DRAM), and analog/mixed-signal integrated circuits. With the scaling down of the device feature size, it is desirable to obtain an ever higher capacitance density. For example, the capacitance density is required to be greater than 10 fF/μm^2 according to the 2020 node of the International Technology Roadmap for Semiconductors (ITRS) [1]. As a consequence, a large number of high-κ materials have been investigated, such as HfO_2 [2–6], ZrO_2 [7–14], Ta_2O_5 [15–18], and TiO_2 [19–24]. Among these high-κ materials, ZrO_2 has a dielectric constant (κ) of 16~25 (monoclinic phase) and a bandgap of 5.8 eV. However, the κ value of ZrO_2 can be enhanced to 36.8 and 46.6 when it is crystallized into cubic and tetragonal phase, respectively [25]. Hence, the capacitance density can be further increased. The microwave annealing (MWA) technique has been tremendously explored for the dopant activation in silicon [26–28] and the silicide formation [29, 30] due to its lower process temperature compared with conventional thermal processing techniques. In addition, Shih et al. [31] investigated the effect of MWA on electrical characteristics of TiN/Al/TiN/HfO_2/Si MOS capacitors. Some key parameters such as equivalent oxide thickness, interface state density, and leakage current density were all improved.

In this work, the effect of MWA on electrical properties of TaN/$Al_2O_3/ZrO_2/Al_2O_3$/TaN (TaN/A/Z/A/TaN) MIM capacitors is investigated. With the usage of MWA, the permittivity of ZrO_2 is remarkably enhanced and the leakage current density is slightly increased. Moreover, the underlying conduction mechanism is also studied.

Methods

Firstly, a 500-nm-thick SiO_2 film was grown onto Si substrate by PECVD, followed by deposition of TaN (20 nm)/Ta (100 nm) films, and TaN was grown by sputtering Ta target in N_2/Ar plasma. Subsequently, the Si wafer coated with the TaN/Ta films was transferred into the ALD chamber, and the nano-stack of Al_2O_3 (2 nm)/ZrO_2 (20 nm)/Al_2O_3 (2 nm) were deposited at 250 °C. Al_2O_3 and ZrO_2 films were grown from Al $(CH_3)_3/H_2O$ and $[(CH_3)_2N]_4Zr/H_2O$, respectively. It is worth mentioning that an ultrathin Al_2O_3 layer between the bottom TaN

* Correspondence: sjding@fudan.edu.cn; zyfan@fudan.edu.cn
[2]School of Microelectronics, Fudan University, Shanghai 200433, People's Republic of China
[1]Department of Materials Science, Fudan University, Shanghai 200433, People's Republic of China

electrode and the ZrO_2 layer was inserted to restrain the formation of interfacial layer during ALD and post-deposition annealing. Afterwards, the samples were subject to the microwave annealing. MWA was performed in a DSGI octagonal chamber at 5.8 GHz. During annealing, the samples were placed at the middle of the chamber, where the electromagnetic field is most uniform. The in situ temperature of the samples was monitored by a Raytek XR series infrared pyrometer facing the backside of the samples. The power was varied from 700 W to 1400 W with a fixed annealing time of 5 min. Finally, a 100-nm-thick TaN top electrode was formed in turn by reactive sputter, lithography, and reactive ion etching.

The ALD film thicknesses were measured with an ellipsometer (SOPRA GES 5E) and confirmed by transmission electron microscope (TEM). Capacitance-voltage (*C-V*) was measured by a precision impedance analyzer (Agilent 4294A) with a 50 mV AC amplitude. Current-voltage (*I-V*) measurements were performed with a semiconductor device analyzer (Agilent B1500) in a dark box. The bias was applied to the top electrode.

Results and Discussion

The schematic structures of the A/Z/A based MIM capacitor and the MWA chamber are shown in Fig. 1a and b, respectively. Figure 1c exhibits the cross-sectional TEM image of the A/Z/A-based MIM capacitor which is subject to the MWA at 1400 W for 5 min. It is observed that the ZrO_2 layer is fully crystallized and the stacked layers can be distinguished clearly, see the inset. Figure 2a shows the cumulative probability plot of the capacitance density at different annealing power. The results show that the capacitance densities of the MIM capacitors are 7.34, 8.87, 8.96, and 9.06 fF/μm^2 respectively for 0, 700, 1050, and 1400 W at a 50% cumulative probability. Therefore, the capacitance

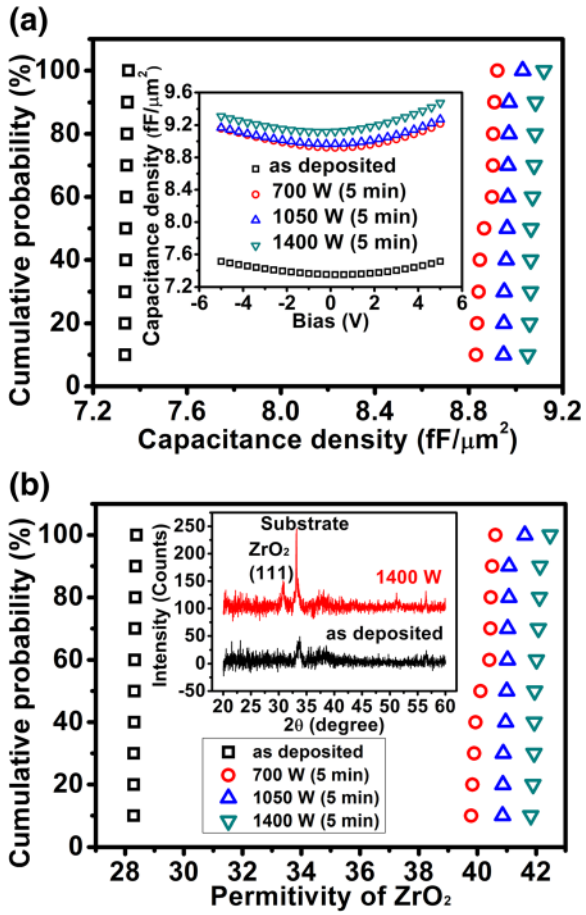

Fig. 2 a The cumulative probability plot of the capacitance density for different samples; the inset displays the capacitance density against the bias. **b** The cumulative probability plot of the permittivity of ZrO_2 for different samples; the inset exhibits the XRD patterns of the as-deposited and 1400 W samples

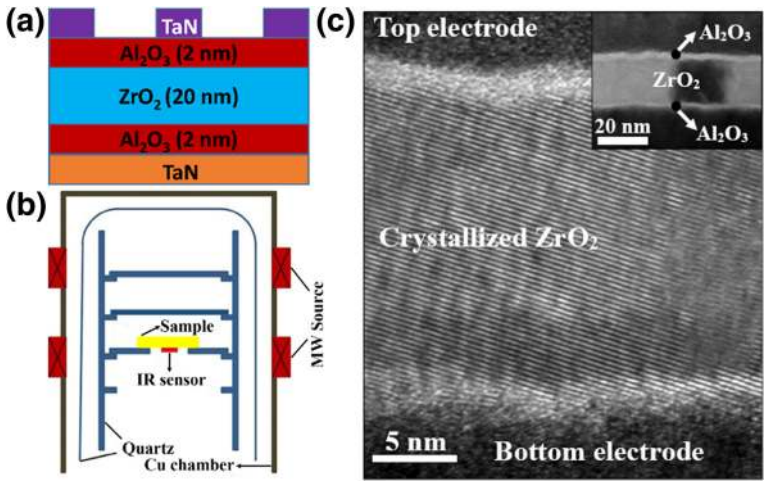

Fig. 1 a The schematic structure of $Al_2O_3/ZrO_2/Al_2O_3$-based MIM capacitor. **b** The schematic structure of the MWA chamber. **c** TEM picture of $Al_2O_3/ZrO_2/Al_2O_3$-based MIM capacitor with MWA at 1400 W for 5 min

density is increased under the effect of microwaves. The very narrow distribution of the capacitance density for the A/Z/A stack MIM capacitors with MWA indicates very good annealing uniformity. The inset in Fig. 2a exhibits the typical CV curves of all the samples. Excluding the effect of Al_2O_3 ($\kappa \approx 8$), the dielectric constants of the ZrO_2 films are extracted as 28.3, 40.1, 41, and 41.9 for 0, 700, 1050, and 1400 W, respectively, revealed by Fig. 2b. Regarding the microwave power of 1400 W, the dielectric constant of the ZrO_2 film increases by 40% compared with the as-deposited sample. The significant enhancement of the permittivity of ZrO_2 can be ascribed to the high-degree crystallization during the microwave annealing, shown in Fig. 1c. As mentioned above, the dielectric constant of ZrO_2 can be enhanced to 36.8 and 46.6 when it is crystallized into cubic and tetragonal phase, respectively [25]. Hence, the XRD measurement was performed to further investigate the mechanism of the dielectric constant enhancement. As exhibited in the inset of Fig. 2b, a peak existed at ~ 30. 7° after the MWA processing at 1400 W, indicating the appearance of the tetragonal phase (111) in ZrO_2 [32, 33]. The presence of this tetragonal phase is responsible for the enhancement of the dielectric constant from 28.3 to over 40.

Since the MIM capacitors are fabricated in the back end of line (BEOL) of integrated circuits, the process temperature must be lower than 400 °C [34]. As shown in Fig. 3, the temperature curves of MWA indicate that the highest temperatures of the substrate are 260, 350, and 400 °C for 700, 1050, and 1400 W, respectively. Therefore, MWA is compatible with the CMOS process from the viewpoint of process temperature. Furthermore, in the previous work [13], Al_2O_3 (2 nm)/ZrO_2 (20 nm)-based MIM capacitors were subject to rapid thermal annealing (RTA) at 420 °C for 10 min in N_2/H_2 ambient and the resulting dielectric constant of ZrO_2 was evaluated as 40. For RTA, the annealing time was kept constant at 420 °C for 10 min, so the thermal budget was much larger compared with MWA. For MWA [35, 36], dipole polarization is thought to be the most important mechanism for energy transfer at the molecular level. When materials in contact have different dielectric properties, microwaves will selectively couple with the higher dielectric loss materials. In contrast, conventional RTA transfers heat most efficiently to materials with high conductivity.

Leakage current is another important parameter for MIM capacitors. As shown by Fig. 4a, the leakage current curve can be divided into two sections for all the samples since there is an obvious turning point, indicating different electron conduction mechanisms. As for the samples with MWA processing, the voltage corresponding to the turning point is smaller compared with the as-deposited sample. Table 1 lists the leakage current density at ± 4 V for all the samples. Take 4 V for example, the leakage current density is increased from 1.06×10^{-7} to 1.92×10^{-5} A/cm^2, i.e., two orders of amplitude enhanced when the microwave power is augmented from 0 to 1400 W. Due to a high crystallization of the ZrO_2 film, a large number of grain boundaries will appear and serve as the leaky path, thus

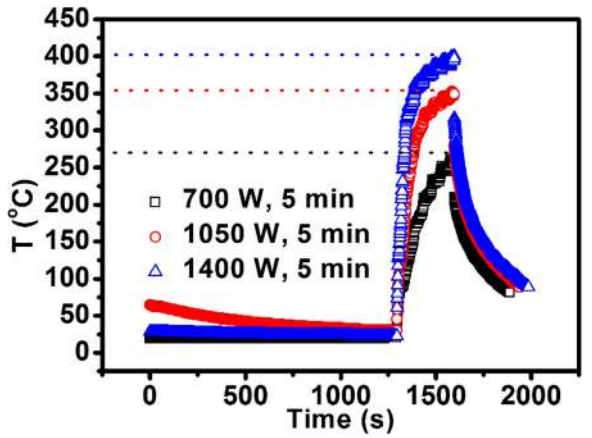

Fig. 3 The curves of the substrate temperature for different samples during the microwave annealing

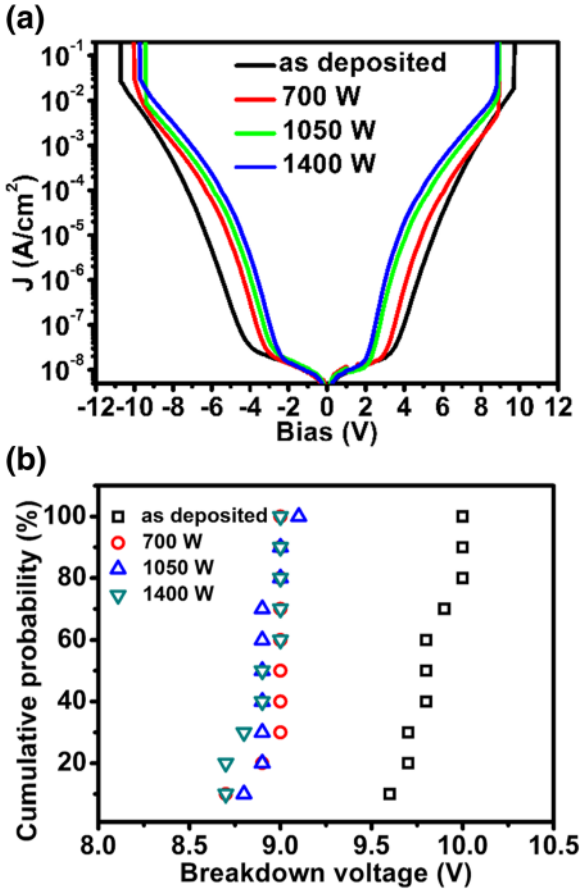

Fig. 4 a The plot of the leakage current density (*J*) vs bias and **b** the cumulative probability plot of the breakdown voltage for different samples

Table 1 The leakage current density (*J*) at ± 4 V for all the samples

	As-deposited	700 W	1050 W	1400 W
J@4 V (A/cm^2)	1.06×10^{-7}	6.68×10^{-7}	7.63×10^{-6}	1.92×10^{-5}
J@-4 V (A/cm^2)	3.41×10^{-8}	3.30×10^{-7}	1.20×10^{-6}	3.48×10^{-6}

enhancing the electron conduction under a high electric field. However, considering a working voltage of 2 V, the leakage current densities are 1.23×10^{-8} and 1.36×10^{-8} A/cm^2 for as-deposited sample and 1400 W sample, respectively. Obviously, the microwave annealing has little effect on the leakage performance under a low electric field. Furthermore, the breakdown voltage was extracted from the *I-V* test and plotted in Fig. 4b. For the as-deposited sample, the breakdown voltage is about 9.8 V at a 50% cumulative probability. With the application of MWA, the breakdown voltage is reduced to ~ 9 V. This reduction of breakdown voltage could be related to the change of the ZrO_2 microstructure.

In order to further understand the effect of MWA on the leakage current, the conduction mechanisms of the MIM capacitors are investigated. Based on the previous research on Al_2O_3 (2 nm)/ZrO_2 (20 nm)-based MIM capacitor [13, 14], the dominant conduction mechanism in a high electric field was confirmed as field-assisted tunneling (FAT). For FAT which is trap-related tunneling, electrons are captured by the traps in the insulator firstly and then tunnel to the conduction band of the insulator directly [37]. In the current work, the Al_2O_3 and ZrO_2 films in the A/Z/A-based MIM capacitors were deposited by the same conditions, so the leakage current is probably predominant by FAT as well. The FAT model can be expressed by Eq. (1) [37]

$$J = AE^2 \exp\left(-\frac{8\pi\sqrt{2m^*q\phi_t^3}}{3hE}\right) \quad (1)$$

where A is a constant, E is the electric field, q is the electronic charge, m^* represents the effective electron mass (about 0.25 m_0, where m_0 is the free electron mass), k is the Boltzmann constant, ϕ_t is the energy barrier separating traps from the conduction band, and h is the Planck's constant.

In terms of the stacked dielectrics, the electric field applied to each layer differs from each other because of different permittivity and thickness. Hence, using the average electric field across the entire stack will bring about severe errors while discussing the conduction mechanism. As a consequence, the electric field across the ZrO_2 layer must be extracted accurately. The electric fields across ZrO_2 are $3.125 \times 10^7 \times V_{stack}$, $2.5 \times 10^7 \times V_{stack}$, $2.47 \times 10^7 \times V_{stack}$, and $2.44 \times 10^7 \times V_{stack}$ respectively for as-deposited, 700 W, 1050 W, and 1400 W sample according to the Gauss law and Kirchhoff voltage law [38, 39]:

$$\begin{cases} k_A E_A = \kappa_Z E_Z \\ d_A E_A + d_Z E_Z = V_{stack} \end{cases} \quad (2)$$

where k_A and κ_Z represent the dielectric constants of Al_2O_3 and ZrO_2, respectively; E_A and E_Z denote the electric fields across Al_2O_3 and ZrO_2, respectively; d_A and d_Z equal the thicknesses of Al_2O_3 and ZrO_2, respectively; and V_{stack} is the voltage applied to the stack. Accordingly, Ln (J/E_Z^2) versus $1/E_Z$ was arbitrarily plotted in Fig. 5, where a straight line fitting was achieved in the high field region for each sample under electron bottom-injection (see Fig. 5a) or electron top-injection (see Fig. 5b). This means that the FAT mechanism is dominated at high electric fields. The extracted ϕ_t is 0.73, 0.51, 0.38, and 0.35 eV respectively for as-deposited, 700 W, 1050 W, and 1400 W sample under electron bottom-injection. In terms of electron top-injection, the corresponding ϕ_t is 0.82, 0.53, 0.47, and 0.43 eV, respectively. Therefore, some shallow traps are induced by MWA. The shallow traps are reported to arise from the grain boundary defects that can introduce additional electronic states near the conduction band [40]. In addition, the conduction mechanism at low fields is most likely trap-assisted tunneling (TAT).

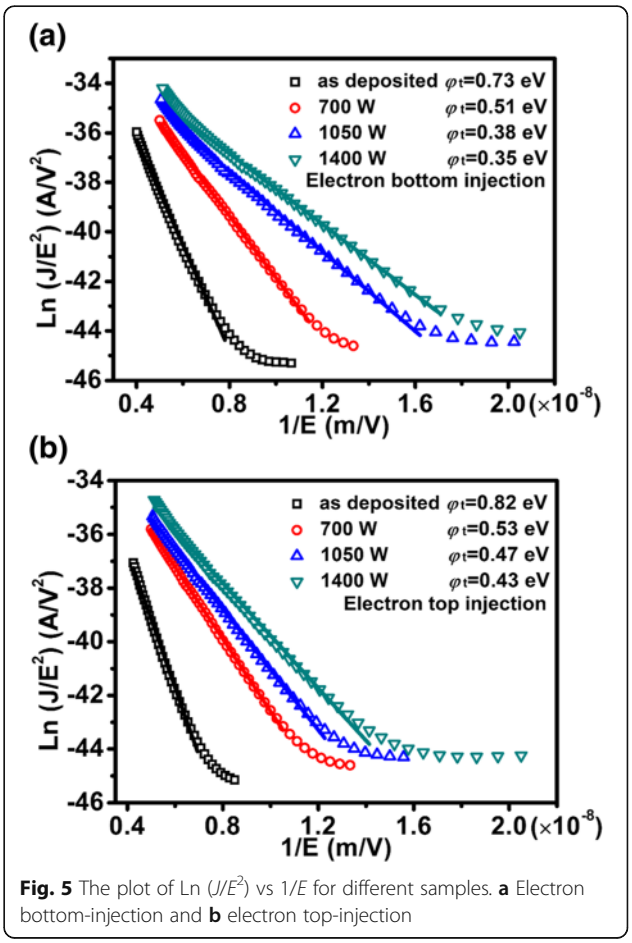

Fig. 5 The plot of Ln (J/E^2) vs $1/E$ for different samples. **a** Electron bottom-injection and **b** electron top-injection

Conclusions

Atomic layer-deposited $Al_2O_3/ZrO_2/Al_2O_3$ nano-stack is used as the insulator of the MIM capacitors. With the effect of MWA at 1400 W for 5 min, the capacitance density is increased to 9.06 fF/μm^2, approximately 23.4% of capacitance enhanced. Decoupling the influence of Al_2O_3, the dielectric constant is deduced as 41.9 for 1400 W sample (~ 40% of permittivity increased). Such enhancement of the permittivity is originated from a high crystallization of the ZrO_2 film. In addition, the substrate temperature is lower than 400 °C, which enables MWA compatible with the BEOL process. This lower substrate temperature can be attributed to the selective heating on the materials of MWA. In terms of a working voltage of 2 V, the leakage current densities are 1.23×10^{-8} and 1.36×10^{-8} A/cm^2 for as-deposited sample and 1400 W sample, respectively. The dominated conduction mechanism in the high electric fields is confirmed as a FAT process. The leakage current in the low electric fields is likely dictated by TAT. Based on the above facts, the microwave annealing is a promising technique used in the CMOS process to enhance the dielectric performance of the MIM capacitors.

Abbreviations

A/Z/A: $Al_2O_3/ZrO_2/Al_2O_3$; ALD: Atomic layer deposition; BEOL: Back end of line; *C-V*: Capacitance-voltage; DRAM: Dynamic random access memory; FAT: Field-assisted tunneling; ITRS: International Technology Roadmap for Semiconductors; *I-V*: Current-voltage; MIM: Metal-insulator-metal; MWA: Microwave annealing; PECVD: Plasma enhanced chemical vapor deposition; RF: Radio frequency; RTA: Rapid thermal annealing; TAT: Trap-assisted tunneling; TEM: Transmission electron microscope

Acknowledgements

There is no acknowledgement.

Funding

This work was supported by the National Key Technologies R&D Program of China (2015ZX02102–003), the National Natural Science Foundation of China (61474027) and the Project funded by China Postdoctoral Science Foundation.

Availability of Data and Materials

All datasets are presented in the main paper and freely available to any scientist wishing to use them for non-commercial purposes, without breaching participant confidentiality.

Authors' Contributions

BZ carried out the main part of fabrication and analytical works. XW and WJL participated in the sequence alignment and drafted the manuscript. SJD, DWZ, and ZF conceived the study and participated in its design. All authors read and approved the final manuscript.

Competing Interests

The authors declare that they have no competing interests.

Publisher's Note

Received: 30 November 2018 Accepted: 21 January 2019
Published online: 11 February 2019

References

1. The International Technology Roadmap for Semiconductors (ITRS) (Semiconductor Industry Association, 2013) Table RFAMS4 On-Chip Passives Technology Requirements. http//public.itrs.net
2. Yu X, Zhu C, Hu H et al (2003) A high-density MIM capacitor (13 fF/μm^2) using ALD HfO_2 dielectrics. IEEE Electr Device L 24:63–65
3. Ding SJ, Zhang DW, Wang LK (2007) Atomic-layer-deposited Al_2O_3-HfO_2 laminated and sandwiched dielectrics for metal-insulator-metal capacitors. J Phys D Appl Phys 40:1072–1076
4. Ding SJ, Zhu C, Li MF et al (2005) Atomic-layer-deposited Al_2O_3-HfO_2-Al_2O_3 dielectrics for metal-insulatormetal capacitor applications. Appl Phys Lett 87:053501
5. Ding SJ, Hu H, Lim HF et al (2003) High-performance MIM capacitor using ALD high-κ HfO_2-Al_2O_3 laminate dielectrics. IEEE Electr Device L 24:730–732
6. Ding SJ, Huang YJ, Li Y et al (2006) Metal-insulator-metal capacitors using atomic-layer-deposited $Al_2O_3/HfO_2/Al_2O_3$ sandwiched dielectrics for wireless communications. J Vac Sci Technol B 24:2518–2522
7. Lee SY, Kim H, McIntyre PC et al (2003) Atomic layer deposition of ZrO_2 on W for metal-insulator-metal capacitor application. Appl Phys Lett 82:2874–2876
8. Kwon HM, Han IS, Park SU et al (2011) Conduction mechanism and reliability characteristics of a metal-insulator-metal capacitor with single ZrO_2 layer. Jpn J Appl Phys 50:04DD02
9. Bertaud T, Bermond C, Blonkowski S et al (2012) Electrical characterization of advanced MIM capacitors with ZrO_2 insulator for high-density packaging and RF applications. IEEE Trans Compon Packag Manuf Technol 2:502–509
10. Bertaud T, Blonkowski S, Bermond C et al (2010) Frequency effect on voltage linearity of ZrO_2-based RF metal-insulator-metal capacitors. IEEE Electr Device L 31:114–116
11. Wu YH, Kao CK, Chen BY et al (2008) High density metal-insulator-metal capacitor based on $ZrO_2/Al_2O_3/ZrO_2$ laminate dielectric. Appl Phys Lett 93:033511
12. Zhang QX, Zhu B, Ding SJ et al (2014) Full ALD $Al_2O_3/ZrO_2/SiO_2/ZrO_2/Al_2O_3$ stacks for high-performance MIM capacitors. IEEE Electr Device L 35:1121–1123
13. Zhu B, Liu WJ, Wei L et al (2015) Voltage linearity modulation and polarity dependent conduction in metal-insulator-metal capacitors with atomic-layer-deposited $Al_2O_3/ZrO_2/SiO_2$ nano-stacks. J Appl Phys 118:014501
14. Zhu B, Liu WJ, Wei L et al (2016) Voltage-dependent capacitance behavior and underlying mechanisms in metal-insulator-metal capacitors with Al_2O_3-ZrO_2-SiO_2 nano-laminates. J Phys D Appl Phys 49:135106
15. Tu YL, Lin HL, Chao LL et al (2003) Characterization and comparison of high-k metal-insulator-metal (MiM) capacitors in 0.13 μm cu BEOL for mixed-mode and RF applications. Symposium on VLSI Technology, pp 79–80
16. Jeong YK, Won SJ, Kwon DJ et al (2004) High quality high-k MIM capacitor by $Ta_2O_5/HfO_2/Ta_2O_5$ multi-layered dielectric and NH_3 plasma Interface treatments for mixed-signal/RF applications. Symposium on VLSI Technology, pp 222–223
17. Thomas M, Farcy A, Perrot C et al (2007) Reliable 3D damascene MIM architecture embedded into Cu interconnect for a Ta_2O_5 capacitor record density of 17 fF/μm^2. Symposium on VLSI Technology, pp 58–59
18. Yang MY, Huang CH, Chin A et al (2003) Very high density RF MIM capacitors (17 fF/μm^2) using high-κ Al_2O_3 doped Ta_2O_5 dielectrics. IEEE Microw Wirel Co 13:431–433
19. Cheng CH, Lin SH, Jhou KY et al (2008) High density and low leakage current in TiO_2 MIM capacitors processed at 300 °C. IEEE Electr Device L 29:845–847
20. Wu YH, Ou WY, Lin CC et al (2012) MIM capacitors with crystalline-TiO_2/SiO_2 stack featuring high capacitance density and low voltage coefficient. IEEE Electr Device L 33:104–106
21. Lin SH, Chiang KC, Chin A et al (2009) High-density and low-leakage-current MIM capacitor using stacked TiO_2/ZrO_2 insulators. IEEE Electr Device L 30:715–717
22. Wu JR, Wu YH, Lin CC et al (2012) Effect of nitrogen passivation on the performance of MIM capacitors with a crystalline-TiO_2/SiO_2 stacked insulator. IEEE Electr Device L 33:878–880
23. Yu MT, Chen KY, Chen YH (2015) TiO_2-based MIM capacitors featuring suppressed leakage current by embedding Ge nanocrystals. RSC Adv 5:13550–13554

24. Woo JC, Chun YS, Joo YH et al (2012) Low leakage current in metal-insulator-metal capacitors of structural $Al_2O_3/TiO_2/Al_2O_3$ dielectrics. Appl Phys Lett 100:081101
25. Zhao X, Vanderbilt D (2001) Phonons and lattice dielectric properties of zirconia. Phys Rev B 65:075105
26. Zhao Z, Theodore ND, Vemuri RNP et al (2013) Effective dopant activation via low temperature microwave annealing of ion implanted silicon. Appl Phys Lett 103:192103
27. Xu P, Fu C, Hu C et al (2013) Ultra-shallow junctions formed using microwave annealing. Appl Phys Lett 102:122114
28. Hou FJ, Sung PJ, Hsueh FK et al (2016) 32-nm multigate Si-nTFET with microwave-annealed abrupt junction. IEEE T Electron Dev 63:1808–1813
29. Hu C, Xu P, Fu C et al (2012) Characterization of Ni (Si,Ge) films on epitaxial SiGe(100) formed by microwave annealing. Appl Phys Lett 101:092101
30. Wu CT, Lee YJ, Hsueh FK et al (2014) Characterization of ultra-thin Ni silicide film by two-step low temperature microwave anneal. ECS J Solid State Sc 3: 122–125
31. Shih TL, Su YH, Kuo TC et al (2017) Effect of microwave annealing on electrical characteristics of TiN/Al/TiN/HfO_2/Si MOS capacitors. Appl Phys Lett 111:012101
32. Tsai CY, Chiang KC, Lin SH (2010) Improved capacitance density and reliability of high-κ Ni/ZrO_2/TiN MIM capacitors using laser-annealing technique. IEEE Electr Device L 31:749–751
33. Monaghan S, Cherkaoui K, O'Connor É (2009) TiN/ZrO_2/Ti/Al metal-insulator-metal capacitors with subnanometer CET using ALD-deposited ZrO_2 for DRAM applications. IEEE Electr Device L 30:219–221
34. Farcy A, Carpentier JF, Thomas M et al (2008) Integration of high performance RF passive modules (MIM capacitors and inductors) in advanced BEOL. Microelectron Eng 85:1940–1946
35. Thostenson ET, Chou TW (1999) Microwave processing: fundamentals and applications. Compos Part A-Appl S 30:1055–1071
36. Fu C, Wang Y, Xu P et al (2017) Understanding the microwave annealing of silicon. AIP Adv 7:035214
37. Lim KY, Park DG, Cho HJ et al (2002) Electrical characteristics and thermal stability of n^+ polycrystalline-Si/ZrO_2/SiO_2/Si metal-oxide-semiconductor capacitors. J Appl Phys 91:414–419
38. Chaneliere C, Autran JL, Devine RAB (1999) Conduction mechanisms in Ta_2O_5/SiO_2 and Ta_2O_5/Si_3N_4 stacked structures on Si. J Appl Phys 86:480–486
39. Mahapatra R, Chakraborty AK, Poolamai N et al (2007) Leakage current and charge trapping behavior in TiO_2/SiO_2 high-κ gate dielectric stack on 4H-SiC substrate. J Vac Sci Technol B 25:217–223
40. McKenna K, Shluger A, Iglesias V et al (2011) Grain boundary mediated leakage current in polycrystalline HfO_2 films. Microelectron Eng 88: 1272–1275